Methanol Synthesis Catalysts

DOI: 10.1002/anie.200702600

Role of Lattice Strain and Defects in Copper Particles on the Activity of $Cu/ZnO/Al_2O_3$ Catalysts for Methanol Synthesis **

Igor Kasatkin, Patrick Kurr, Benjamin Kniep, Annette Trunschke, and Robert Schlögl*

Dedicated to Süd-Chemie on the occasion of its 150th anniversary

Copper-based catalysts are industrially applied in various reactions, including the water–gas shift reaction, synthesis of fatty alcohols from fatty acid methyl esters, and methanol synthesis. Today, methanol is produced at low pressures (35–55 bar) and 200–300 °C over $Cu/ZnO/Al_2O_3$ catalysts.[1] Owing to their great commercial relevance, Cu/ZnO-based catalysts have been extensively studied, and many different models have been proposed regarding the nature of active sites and the valence of copper during methanol formation, such as copper(I) dispersed in ZnO,[2,3] metallic copper supported on ZnO,[4] dynamic surface and bulk alloy formation depending on the reduction potential of the synthesis gas,[5,6] modification of the surface chemistry of ZnO due to charge transfer from zinc oxide to Cu,[7] and ZnO segregated on copper(I).[8] The catalytic activity of the binary catalyst has been reported to be several orders of magnitude greater than that of either metallic Cu or pure ZnO, thus indicating a synergetic interaction of the two components.[9] ZnO is regarded either as a provider of atomic spillover hydrogen for further hydrogenation of adsorbed reaction intermediates on Cu sites[10,11] or as a structure-directing support controlling dispersion, morphology, and specific activity of the metal particles.[12–18] Strong interaction between the metal and the support, especially in the case of a large lattice mismatch, is known to cause strain in the metal particles, to which an increase in catalytic performance has been attributed.[19–21] On the other hand, one-monolayer and thicker Cu islands epitaxially grown on the ZnO $(000\bar{1})$ surface were experimentally found to be strain-free.[22]

Most earlier studies have investigated model catalysts with low Cu loadings ($Cu/Zn \ll 1$) containing large ZnO single crystals, although in commercial catalysts copper usually represents the main component ($Cu/Zn > 1$) and the ZnO particles, acting as spacers rather than as supports, are comparable in size to or even smaller than the Cu particles. Herein, we report the results of TEM and in situ XRD characterization of a series of $Cu/ZnO/Al_2O_3$ catalysts exhibiting different catalytic activities. The molar ratio Cu/Zn/Al = 60:30:10 is characteristic of commercial catalysts.[1] The microstructural features of the materials prepared by coprecipitation with sodium carbonate from metal nitrate solution are analyzed after calcination in air at 330 °C and subsequent reduction in hydrogen at 250 °C.

The TEM and high-resolution TEM images shown in Figure 1 illustrate the microstructure typical of these catalysts. Generally, 10 to 15 clusters similar to the one shown in Figure 1a with sizes varying from 100 nm to several micrometers were analyzed in each of the catalysts with energy-dispersive X-ray spectroscopy (EDX) to determine the concentrations of Al, Cu, and Zn. The average values (Al 10.6 ± 4.5, Cu 62.7 ± 7.2, Zn 26.7 ± 4.2 atom %) are close to the nominal composition. Figure 2, which contains data of catalysts, illustrates the scattering that is due to local inhomogeneities.

The particles of Cu and ZnO in the activated state of the catalyst form a porous framework (Figure 1b). The ZnO particles serve as spacers between the Cu particles, preventing them from sintering. Frequently, the Cu particles are in contact with several ZnO particles. The copper surface is partially or completely covered by ZnO (Figure 1c,d) and thus less accessible to the reacting molecules. As is evident from the images in Figure 1, most Cu particles exhibit a rounded (non-equilibrium) shape that is similar to that of an ellipsoid or sphere; these shapes are sometimes truncated with {111} or {100} facets. The mean Cu particle size was determined by measuring projected areas of individual particles in the TEM images and calculating the equivalent diameter, which corresponds to the diameter of a circle with the same area. Statistical tests showed that the mean sizes were significantly different in different clusters and depended on the elemental composition (data not shown). Redundant measurements were performed to check that further increase in the number of measured particles changed neither the mean size nor the shape of the distribution curve. The total number of measured particles varied from 5060 to 24200 in different samples. Because ZnO and Al_2O_3 display a lower degree of crystallinity than Cu, the oxide particles were not well-shaped and separated from one another. This prevented accurate determination of their mean size in TEM projections.

[*] Dr. I. Kasatkin, Dipl.-Ing. P. Kurr, Dr. A. Trunschke, Prof. Dr. R. Schlögl
Department of Inorganic Chemistry
Fritz Haber Institute of the Max Planck Society
Faradayweg 4–6, 14195 Berlin (Germany)
Fax: (+49) 30-8413-4405
E-mail: trunschke@fhi-berlin.mpg.de
Dr. B. Kniep
Süd-Chemie AG
R&D Catalysts
Waldheimer Str. 13, 33052 Bruckmühl (Germany)

[**] The authors are grateful to Prof. Dr. Thorsten Ressler, Technical University Berlin, for fruitful discussions. We acknowledge the Federal Ministry of Education and Research (FKZ 01RI0529) and the Deutsche Forschungsgemeinschaft (SPP 1051) for financial support.

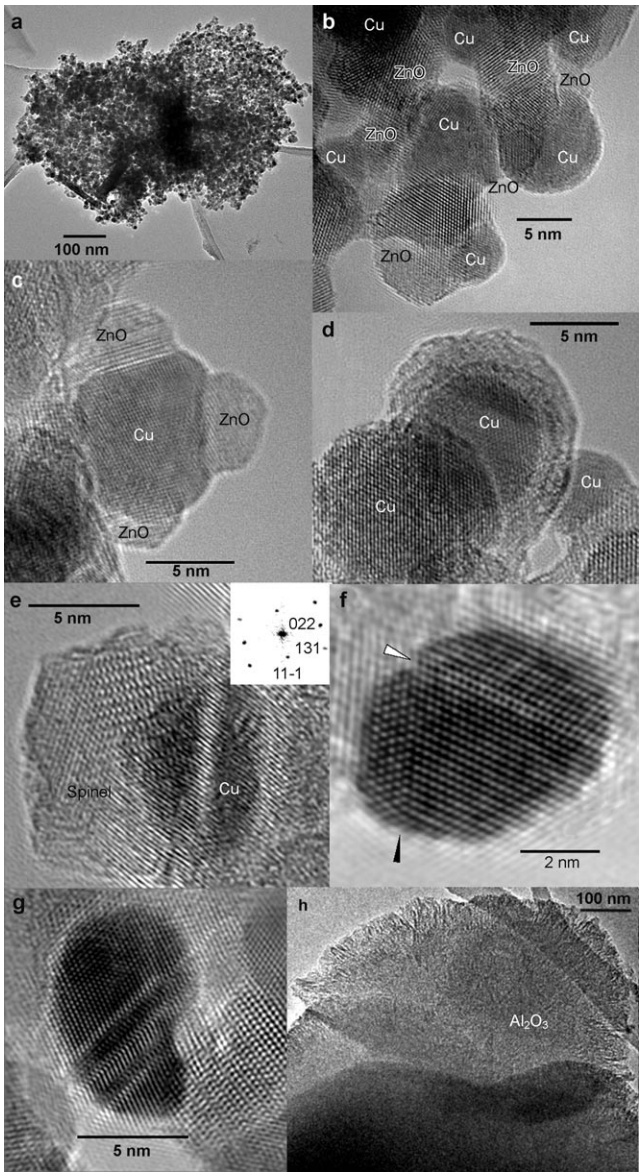

Figure 1. Microstructural features revealed with TEM and high-resolution TEM. See text for details.

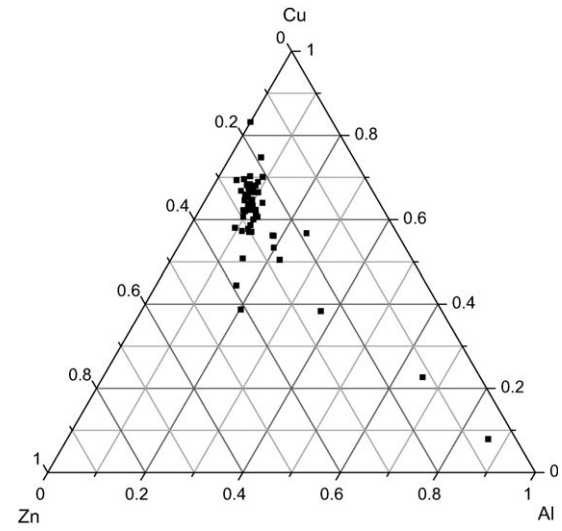

Figure 2. Elemental distribution determined by EDX analyses.

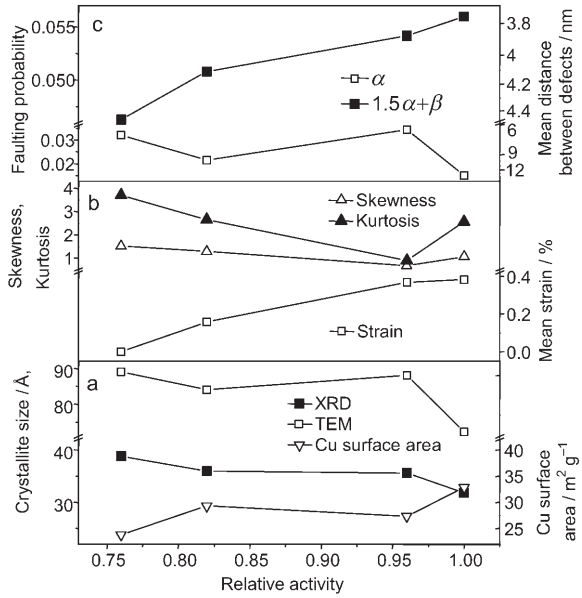

Figure 3. Microstructural parameters obtained with TEM and XRD as a function of relative catalytic activity in methanol synthesis. The errors for all the values plotted (standard errors for the mean particle size determined with TEM) are within the size of the corresponding symbols, except for the strain; see text for details.

Figure 3a demonstrates that the mean Cu particle size measured by TEM (□) is not related to the catalytic activity in methanol synthesis. Based on the results of EDX analyses and the particle size measurements, the mean specific Cu surface area was determined in each of the samples studied (Figure 3a, ▽). In those calculations, the decrease in the fraction of open surface with decreasing particle size (owing to the stronger wetting of small particles) was taken into account, but the coverage of the Cu surface by smaller ZnO particles was not (Figure 1c,d). Accurate determination of gas-accessible Cu surface area using two-dimensional TEM projections was impossible. However, consistent copper surface areas have been measured by N_2O chemisorption for two of the catalysts. Therefore, the values based on TEM are considered to be representative for the copper surface areas accessible to the gas phase. As expected, the calculated mean surface area is inversely proportional to the mean particle size. A correlation between copper surface area and catalytic activity is not observed, but the most active catalyst possesses the largest surface area and the least active the smallest.

As seen in Figure 3b, with the exception of the most active material, the degree of asymmetry (skewness) and the kurtosis of the particle size distribution decrease with increasing catalytic activity. In other words, with increasing activity, the particle size distribution approaches the Gaussian law. A pronounced log-normality, that is, asymmetry of the particle size distribution measured with TEM, may result

from sintering of smaller Cu particles, which, in turn, may be considered as an indication of the nonoptimal microstructure of the material. As seen in the Figure 3b, a more symmetric size distribution results in increased activity; on the other hand, a material with asymmetric distribution demonstrated the highest activity, which could be associated with considerably smaller mean Cu particle size and, correspondingly, higher specific Cu surface area. However, ineffective interaction with the ZnO spacer resulted in a higher tendency towards sintering in the latter material.

Alumina is present in two structures. It tends to segregate, and it occurs in mixed-oxide particles. Agglomerated masses of amorphous material, comparable in size to clusters of Cu/ZnO nanoparticles but containing only traces of Cu and Zn, were observed (Figure 1h). Furthermore, amorphous or poorly crystallized alumina was intermixed with Cu and ZnO particles. In rare cases, HRTEM images reveal small regions of better-crystallized particles (Figure 1e). The corresponding power spectrum (Figure 1e, inset) allowed identification of a spinel-like cubic structure with the lattice distances d_{111}, d_{311}, d_{220} markedly closer to those of $ZnAl_2O_4$ (ICDD 5-669) than of pure cubic Al_2O_3 (ICDD 47-1292). Positive correlations between the concentration of Al and Zn determined with EDX in different clusters within all samples support the hypothesis on the formation of $ZnAl_2O_4$ spinel.

Most of the Cu particles, especially those larger than 5 nm, contained various defects, the most typical of which were twins and stacking faults (Figure 1e–g). Many particles demonstrated multiple twinning along a certain octahedral plane (Figure 1g), but only a few decahedral and no icosahedral cyclic twins were found. Characteristically, most of the twin boundaries were only partially coherent, that is, the regular close packing of the octahedral planes was interrupted by missing a layer in the direction normal to the twin boundary. Coherent and partially coherent twin boundaries are marked in Figure 1f with the black and white arrows, respectively.

To evaluate both crystallite size and strain, the profiles of the 111 and 222 reflections of Cu were simulated simultaneously with the same set of model parameters. Strain was introduced into the model as a Gaussian distribution of the interplanar distances around the mean value of $d_{111} = 2.088$ Å. The standard deviation of the distribution expressed in percent of d_{111} was used as a quantitative measure of strain. Because of the poor quality of Cu 222 reflections, the absolute values of strain plotted in Figure 3b could only be roughly estimated with the accuracy of about $\pm 10\%$. The mean crystallite size calculated from diffraction peak broadening (Figure 3a, ■) is invariably smaller than the particle size measured with TEM (Figure 3a, □). The presence of stacking faults and twin boundaries in the particles (Figure 1f,g) may account for the discrepancy.[23] The stacking-fault probability α could be determined from the measurements of intervals between the adjacent peaks in the XRD patterns in such pairs as 111–200, which are known to progressively shift in opposite directions as α increases, and comparing them to the corresponding intervals in a "perfect" material using equations given by Warren.[23]

Accordingly, the stacking-fault probability α was found to change in the series of studied materials as shown in Figure 3c. The right-hand axis shows the mean distance between the defects calculated as $l = d_{111}/\alpha$ or $l = d_{111}/(1.5\,\alpha+\beta)$, where β is the twinning probability. The overall faulting probability $1.5\,\alpha + \beta$ could be estimated from the comparison of apparent crystallite sizes determined by the shape analysis of different peaks. However, the low signal-to-noise ratio of XRD reflections other than 111 made their detailed analysis unreliable. Therefore, a combined analysis of XRD and TEM data was undertaken based on the assumption that the presence of stacking faults and twin boundaries is the only reason for the smaller domain size determined by XRD analysis of the Cu 111 reflection compared to the mean particle size determined by TEM. In addition, a nearly spherical shape of the Cu particles is assumed, which is supported by the TEM images (Figure 1). The upper curve in Figure 3c shows the trend in the overall faulting probability in the studied catalysts obtained by the combined treatment of the series of TEM and XRD data.

Inspection of Figure 3 shows that the stacking fault probability α does not correlate with the activity but changes in parallel with the TEM particle size, whereas the mean distance between stacking faults is comparable to the mean particle size (8.1 and 8.3 nm, respectively). This result does not necessarily imply that there is a physical reason preventing small particles from faulting. The effect can be interpreted from a geometrical point of view. At a given mean distance between the defects, the larger particles are more likely to contain defects than the smaller ones.

At the same time, the independent measurements show that the activity is proportional to the overall faulting probability $1.5\,\alpha + \beta$. The assignment of the spots where twin boundaries meet the surface as active sites remains speculative despite the trends in Figure 3, as substantial simplifications are involved in estimating the defect properties based on the combined analysis of XRD and TEM data.

The activity is, however, clearly related to the strain in Cu crystallites (Figure 3b). The correlation between the mean strain and the overall faulting probability does not allow us to distinguish between the effects of specific atomic configurations produced on the particle surface by twin boundaries and stacking faults and the effects of the strain itself, which is associated with these defects. Nevertheless, this correlation clearly shows the essential role of imperfections in the Cu lattice for the increased activity of $Cu/ZnO/Al_2O_3$ catalysts in methanol synthesis. At the given small size of the Cu particles, most lattice defects occurring in the bulk of the metal will terminate at the surface and hence become effective for catalytic purposes. For sustained function, these defects must remain pinned under working conditions by chemical impurities or interfacial strain. For both effects, ZnO is instrumental in giving one hint towards the explanation of the synergy between Cu and ZnO.

In summary, the statistically meaningful analysis of the nanostructure of a series of catalysts for methanol synthesis with compositions close to technical systems has revealed that the abundance of non-equilibrium structures in Cu, such as planar defects and strain (which are strongly interrelated),

clearly correlate with catalytic activity. The families of correlations suggested by Muhler and co-workers[24] may find their physical interpretation in the distribution functions of nanostructural properties as evidenced in Figure 3. We speculate that the relevant non-equilibrium structure of active Cu is generated during synthesis, thus leaving either Zn from the mixed metal hydroxycarbonate in the copper or leaving oxygen from the oxide–suboxide reduction sequence dissolved in Cu. This situation can explain the observation of the chemical memory.[25] The kinetic stabilization of metastable structures during long-term operation is seen as the physical reason for the synergy, as suggested much earlier.[11] The synthesis of Cu-based catalysts can now be redesigned to optimize their exact chemical composition (Figure 2), Cu particle size distribution function (Figure 3), and the abundance of stabilizing species at Cu interfaces (Figure 1). We suggest that stabilized planar defects in nanostructured Cu, through their termination features at the surface, create unique geometric and electronic situations, thus allowing active sites to form. In this non-obvious way, bulk real structure, nanostructuring, and surface catalytic function are interlinked, forming a bridge over the material gap between equilibrated and highly active forms of Cu metal.

Experimental Section

A Philips CM200FEG microscope operated at 200 kV and equipped with a field emission gun and the Gatan imaging filter was used. The coefficient of spherical aberration was $C_s = 1.35$ mm. The information limit was better than 0.18 nm. High-resolution images with a pixel size of 0.016 nm were taken at a magnification of 1083000× with a CCD camera, and selected areas were processed to obtain the power spectra (square of the Fourier transform of the image). The power spectra were used for measuring interplanar distances (±0.5%) and angles (±0.5 deg) for phase identification.

The XRD data in the 2θ range of 10–100° were collected on a STOE Theta/theta X-ray diffractometer ($Cu_{K\alpha}$ radiation, secondary graphite monochromator, scintillation counter, 2θ step 0.04°, counting time 5 s) equipped with an Anton Paar XRK 900 in situ reactor chamber. The in situ reduction was performed at 250 °C (heating rate 2 °C min^{-1}) in 2% H_2/N_2.

The profiles of the Cu 111 and 222 reflections measured by in situ X-ray diffraction were analyzed within the 2θ intervals 38–49° and 90–100°, respectively, after the neighboring peaks had been fitted with pseudo-Voigt functions and their contributions subtracted. A comparison with the XRD pattern of LaB_6 (NIST standard SRM 660a) obtained under the same conditions showed that the effect of size/strain peak broadening dominated over instrumental effects such that the latter could be safely neglected.

An adopted model was used to simulate the peak profiles from first principles by double summation of interference functions over different column lengths and over different lattice spacings according to the corresponding distribution functions.[26] A trial-and-error procedure was used to determine approximate values, which were further refined with a least-square procedure in the final step. As opposed to similar models,[27] the applied model did not impose any restrictions on the laws of both lattice spacing and crystallite size distribution (normal, log-normal, etc.). The size-distribution shape was described by a polynomial function whose coefficients were refined during simulation. The flexibility in defining nonstandard or polymodal size distributions allowed highly precise simulation of the XRD peak shape. All of the values plotted in Figure 3, which were calculated from the analysis of the shape of the Cu 111 reflection and from the shifts of the Cu 111 and 200 reflections, have errors smaller than the size of corresponding symbols.

The catalysts were tested at a temperature of 483 K and a pressure of 60 bar. The feed was composed of 72% H_2, 10% CO, 4% CO_2, and 14% He.

Received: June 14, 2007
Revised: July 26, 2007

Keywords: aluminum · copper · electron microscopy · methanol synthesis · zinc

[1] P. J. A. Tijm, F. J. Waller, D. M. Brown, *Appl. Catal. A* **2001**, *221*, 275–282.
[2] K. Klier, *Adv. Catal.* **1982**, *31*, 243–313.
[3] V. Ponec, *Surf. Sci.* **1992**, *272*, 111–117.
[4] K. C. Waugh, *Catal. Today* **1992**, *15*, 51–75.
[5] N.-Y Topsøe, H. Topsøe, *Top. Catal.* **1999**, *8*, 267–270.
[6] Y. Choi, K. Futagami, T. Fujitani, J. Nakamura, *Appl. Catal. A* **2001**, *208*, 163–167.
[7] J. C. Frost, *Nature* **1988**, *334*, 577–580.
[8] W. P. A. Jansen, J. Beckers, J. C. v. d. Heuvel, A. W. Denier v. d. Gon, A. Bliek, H. H. Brongersma, *J. Catal.* **2002**, *210*, 229–236.
[9] R. G. Herman, K. Klier, G. W. Simmons, B. P. Finn, J. B. Bulko, *J. Catal.* **1979**, *56*, 407–429.
[10] R. Burch, S. E. Golunski, M. S. Spencer, *J. Chem. Soc. Faraday Trans.* **1990**, *86*, 2683–2691.
[11] M. S. Spencer, *Catal. Lett.* **1998**, *50*, 37–40.
[12] J. Yoshihara, C. T. Campbell, *J. Catal.* **1996**, *161*, 776–782.
[13] C. V. Ovesen, B. S. Clausen, J. Schiøtz, P. Stoltze, H. Topsøe, J. K. Nørskov, *J. Catal.* **1997**, *168*, 133–142.
[14] T. Fujitani, J. Nakamura, *Catal. Lett.* **1998**, *56*, 119–124.
[15] N.-Y. Topsoe, H. Topsoe, *J. Mol. Catal. A* **1999**, *141*, 95–105.
[16] J. D. Grunwaldt, A. M. Molenbroek, N.-Y. Topsøe, H. Topsøe, B. S. Clausen, *J. Catal.* **2000**, *194*, 452–460.
[17] P. L. Hansen, J. B. Wagner, S. Helveg, J. R. Rostrup-Nielsen, B. S. Clausen, H. Topsøe, *Science* **2002**, *295*, 2053–2055.
[18] R. A. Hadden, B. Sakakini, J. Tabatabaei, K. C. Waugh, *Catal. Lett.* **1997**, *44*, 145–151.
[19] M. M. Günter, T. Ressler, B. Bems, C. Büscher, T. Genger, O. Hindrichsen, M. Muhler, R. Schlögl, *Catal. Lett.* **2001**, *71*, 37–44.
[20] M. M. Günter, T. Ressler, R. E. Jentoft, B. Bems, *J. Catal.* **2001**, *203*, 133–149.
[21] J. B. Wagner, P. L. Hansen, A. M. Molenbroek, H. Topsøe, B. S. Clausen, S. J. Helveg, *J. Phys. Chem. B* **2003**, *107*, 7753–7758.
[22] N. Jedrecy, S. Gallini, M. Sauvage-Simkin, R. Pinchaux, *Phys. Rev. B* **2001**, *64*, 085424.
[23] B. E. Warren, *X-ray Diffraction*, Dover Publications, New York, **1990**.
[24] M. Kurtz, N. Bauer, C. Büscher, H. Wilmer, O. Hinrichsen, R. Becker, S. Rabe, K. Merz, M. Driess, R. A. Fischer, M. Muhler, *Catal. Lett.* **2004**, *92*, 49–52.
[25] B. Bems, M. Schur, A. Dassenoy, H. Junkes, D. Herein, R. Schlögl, *Chem. Eur. J.* **2003**, *9*, 2039–2052.
[26] I. A. Kasatkin, T. I. Ivanova, *Crystallogr. Rep.* **1998**, *43*, 1015–1019.
[27] F. Sánchez-Bajo, A. L. Ortiz, F. L. Cumbrera, *Acta Mater.* **2006**, *54*, 1–10.

